

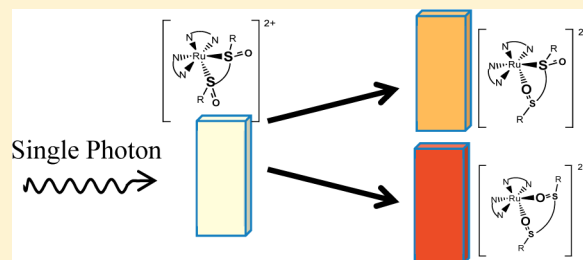
One Photon Yields Two Isomerizations: Large Atomic Displacements during Electronic Excited-State Dynamics in Ruthenium Sulfoxide Complexes

Komal Garg,[‡] Albert W. King,[‡] and Jeffrey J. Rack*

Nanoscale and Quantum Phenomena Institute, Department of Chemistry and Biochemistry, Ohio University, Athens, Ohio 45701, United States

S Supporting Information

ABSTRACT: Photochromic compounds efficiently transduce photonic energy to potential energy for excited-state bond-breaking and bond-forming reactions. A critical feature of this reaction is the nature of the electronic excited-state potential energy surface and how this surface facilitates large nuclear displacements and rearrangements. We have prepared two photochromic ruthenium sulfoxide complexes that feature two isomerization reactions following absorption of a single photon. We show by femtosecond transient absorption spectroscopy that this reaction is complete within a few hundred picoseconds and suggest that isomerization occurs along a conical intersection seam formed by the ground-state and excited-state potential energy surfaces.



INTRODUCTION

Photochromic compounds selectively and specifically transduce photonic energy to potential energy for excited-state bond-breaking and bond-forming reactions. Accordingly, they are of fundamental interest in pursuit of understanding photophysical and photochemical reactions involving the coupling of atomic motions to electronic transitions. Moreover, due to the disparate electronic and molecular structures exhibited by the ground state (GS) and metastable state (MS), they provide a unique chemical environment for investigating how large atomic motions are coupled with electronic transitions. Indeed, photochromic compounds have been the focus of certain computational studies,^{1–11} which are related to a larger class of photochemical reactions, where electronic transitions occur non-adiabatically through conical intersections or conical intersection seams.^{12–19} Photoinduced or phototriggered molecular motions are important design aspects in light-driven molecular machines,^{20–23} in photomechanical effects,^{24–27} in certain photoresponsive materials,^{28–33} and in solar thermal energy storage.^{34–36}

A critical feature of photochromic compounds (and photochemical reactions in general) is the shape and electronic character of the excited-state potential energy surface that promotes bond-breaking and bond-forming reactions. In principle, such knowledge permits optimization of these surfaces through synthetic design with respect to specific parameters, such as temporal response, quantum yield, photoreversibility, or magnitude of color change. Recent reports on concerted multiple *cis–trans* isomerizations in polyenes demonstrate these challenges.^{37,38} We have created a class of photochromic compounds based on a phototriggered isomerism of a coordinated sulfoxide ligand, where the GS is S-

bonded and the MS is O-bonded.^{39–41} Our study of these compounds reveals that the isomerization (time constants ranging from 45 ps to 1.5 ns) and efficiency (quantum yields ranging from 0.03 to 0.9) of the photochemical transformation can be tuned through judicious choice of ligand structure.^{42,43} For example, we recently reported that for $[\text{Ru}(\text{bpy})_2(\text{pySO})]^{2+}$ (bpy = 2,2'-bipyridine; pySO = 2-(isopropylsulfinylmethyl)pyridine), S→O and O→S isomerizations are phototriggered with two different wavelengths of light.⁴⁴ Consistent with this observation, we found that upon irradiation of this complex with white light in solution a photostationary state was produced. In another case, spectroscopic data of $[\text{Ru}(\text{bpy})_2(\text{OSO})]^+$ (OSO = 2-methylsulfinylbenzoate) are consistent with computational results showing that isomerization occurs through a conical intersection.^{2,45} In contrast to the first example above, $[\text{Ru}(\text{bpy})_2(\text{OSO})]^+$ features only a phototriggered S→O isomerization pathway and not a photochemical O→S isomerization. Furthermore, we have investigated a series of bis-sulfoxide complexes with the long-term aim of determining how two isomerizations may be triggered by a single-photon absorption.^{46–50} The fundamental purpose of this study is to reveal the nature of the interaction between the electronic wave function and large atomic displacements. Due to the distinct absorption spectra of these isomers, bis-sulfoxides are ideally suited for observing this interaction. In this article, we show that two sulfoxide isomerizations can be triggered from a single-photon absorption in chelating bis-sulfoxide complexes.

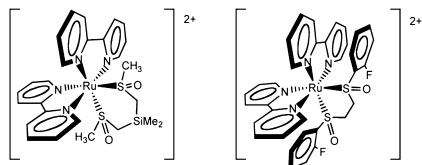
Received: September 6, 2013

Published: January 17, 2014

RESULTS AND DISCUSSION

Shown in Chart 1 are bond line sketches of the two complexes investigated in this study. The compounds, [Ru-

Chart 1. Bond Line Drawings of [Ru(bpy)₂(OSSO)]²⁺ (Left) and [Ru(bpy)₂(F-bpSO)]²⁺ (Right)



(bpy)₂(OSSO)]²⁺, where OSSO = dimethylbis(methylsulfinylmethyl)silane, and [Ru(bpy)₂(F-bpSO)]²⁺, where F-bpSO = 1,2-bis(2-fluorophenyl)sulfanyl ethane, were produced according to literature procedures.^{46,48,51} Briefly, [Ru(bpy)₂Cl₂] was mixed with the bis-thioether ligand to yield the bis-thioether ruthenium complex, which was subsequently oxidized to the bis-sulfoxide ruthenium complex. Elemental analysis and ¹H NMR spectra are consistent with the formulation of each compound.

The electronic spectra of [Ru(bpy)₂(OSSO)]²⁺ and [Ru(bpy)₂(F-bpSO)]²⁺ are shown in Figures 1a and 2a, respectively. For [Ru(bpy)₂(OSSO)]²⁺, the lowest energy absorption maximum is observed at 355 nm and is assigned to a Ru dπ→bpy π* metal-to-ligand charge-transfer (MLCT) transition on the basis of its position and intensity (ε = 4560 M⁻¹ cm⁻¹). The MLCT absorbance maximum for [Ru(bpy)₂(F-bpSO)]²⁺ appears as a shoulder on the bipyridine-centered π→π* transition at ~340 nm. This shift to the blue for the MLCT transition is due to stabilization of the sulfur lone pair by the aromatic phenyl ring. These MLCT absorption maxima are strongly indicative of Ru dπ orbital stabilization by the sulfoxides.

Irradiation of both [Ru(bpy)₂(OSSO)]²⁺ and [Ru(bpy)₂(F-bpSO)]²⁺ reveals striking changes in their electronic spectra. For [Ru(bpy)₂(OSSO)]²⁺, 400 nm excitation shows a rise in the optical density of the solution resulting in the formation of two new peaks at 350 and 500 nm (Φ_{SS→OO} = 0.28; Figure 1b). In accord with literature precedence, these new absorption maxima are assigned to the bis-O-bonded isomer, in which S→O isomerization of both sulfoxides is triggered by light.^{49,52} For comparison, the closely related [Ru(bpy)₂(OH₂)₂]²⁺ compound (containing two O-atom donors) features absorption maxima of 360 and 498 nm.⁵³ Importantly, only a single isosbestic point is observed, suggesting that the bis-O-bonded isomer is produced from the S,S-ground state without the formation of a ground-state reaction intermediate.

Similarly, 355 nm excitation of [Ru(bpy)₂(F-bpSO)]²⁺ results in the formation of a new isomer with absorption maxima at 360 and 495 nm (Φ_{SS→OO} = 0.10; Figure 2b). Again, we assign this new spectrum to the bis-O-bonded isomer. In accord with [Ru(bpy)₂(OSSO)]²⁺, these bulk photolysis data also show only a single isosbestic point. In both compounds, the spectral changes are reversible at room temperature, with complete re-formation of the ground-state bis-S-bonded isomers occurring over a period of days to weeks. The spectral changes of this transformation are consistent with two sequential O→S isomerizations on the ground-state potential energy surface.

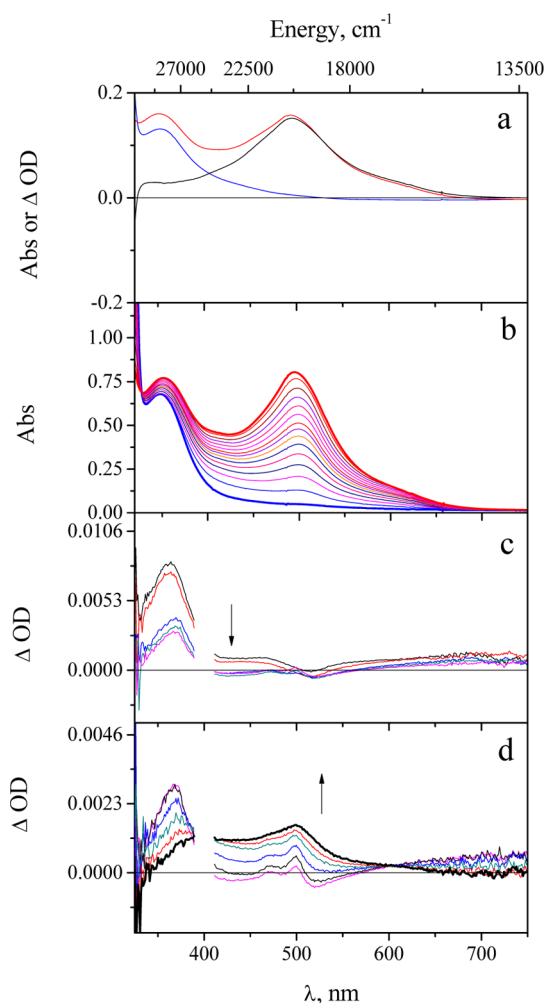


Figure 1. (a) Steady-state electronic spectra of S,S-[Ru(bpy)₂(OSSO)]²⁺ (blue) and O,O-[Ru(bpy)₂(OSSO)]²⁺ (red). The difference trace (black) is obtained from subtraction of the S,S spectrum from the O,O spectrum. (b) Spectral changes in the solution obtained from bulk photolysis of S,S-[Ru(bpy)₂(OSSO)]²⁺ (blue, bottom), producing O,O-[Ru(bpy)₂(OSSO)]²⁺ (red, top). Total irradiation time is 40 min from 400 nm excitation. (c) Transient spectra collected at pump–probe delays of 0.3, 1.0, 5.0, 15, and 65 ps (black to magenta), obtained from magic angle pump excitation at 400 nm. Complex concentration is 1.19 × 10⁻⁴ M. (d) Transient spectra collected at pump–probe delays of 65, 150, 350, 600, 1500, and 2800 ps (magenta to bold black), obtained from magic angle pump excitation at 400 nm.

We employed femtosecond transient absorption spectroscopy to reveal kinetic details of the excited-state reactivity of these compounds. Shown in Figure 1c,d are the early (<65 ps) and late (>65 ps) spectral changes for [Ru(bpy)₂(OSSO)]²⁺ in propylene carbonate at different pump–probe delays following magic angle excitation at 400 nm. Figure 1a also displays the difference spectrum obtained from subtraction of the S,S-isomer from the O,O-isomer (ΔOD = A_{t=t} - A_{t=0} = O,O - S,S). If the O,O-isomer is created following excitation of the S,S-isomer, then this difference spectrum should be observed in the transient spectra. The early time traces (Figure 1c, from 0.3 to 65 ps) show a sharp feature at ~360 nm and a broad excited-state absorption at λ > 600 nm. The data near the excitation wavelength have been removed for clarity. The 360 nm feature has been assigned to a π*→π* absorption of the reduced

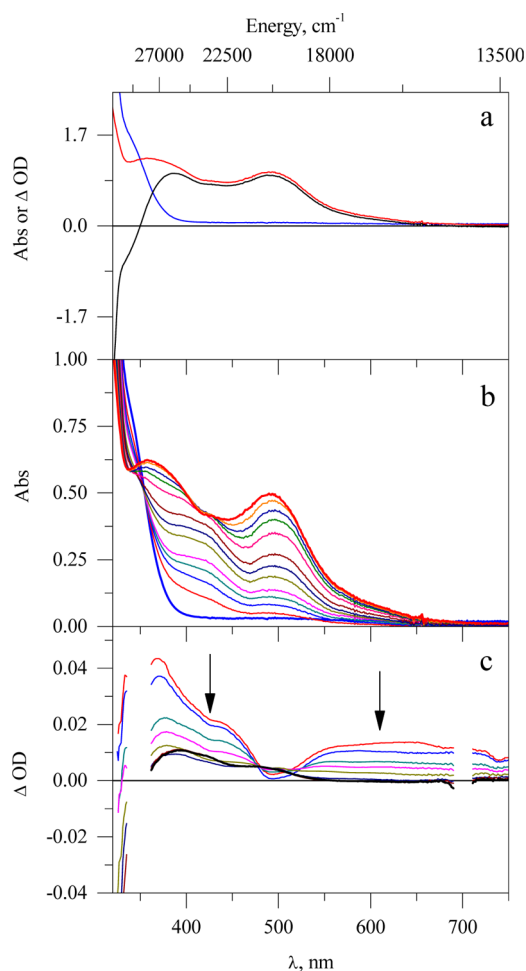


Figure 2. (a) Steady-state electronic spectra of S,S -[Ru(bpy)₂(F-bpSO)]²⁺ (blue) and O,O -[Ru(bpy)₂(F-bpSO)]²⁺ (red). The difference trace (black) is obtained from subtraction of the S,S spectrum from the O,O spectrum. (b) Spectral changes in the solution obtained from bulk photolysis of S,S -[Ru(bpy)₂(F-bpSO)]²⁺ (blue, bottom), producing O,O -[Ru(bpy)₂(F-bpSO)]²⁺ (red, top). Total irradiation time is 30 min from 355 nm excitation. Complex concentration is 1.61×10^{-4} M. (c) Transient spectra collected at pump–probe delays of 0.75, 1.0, 5.0, 10, 20, 75, 500, and 3000 ps (red to bold black).

bipyridine in the MLCT excited state, while the low-energy feature has been previously ascribed to both an LMCT transition from the unreduced bipyridine to Ru(III) and $\pi^* \rightarrow \pi^*$ absorption of the reduced bipyridine.^{54,55} The sharp, negative peaks near 500 nm are due to stimulated emission, as the S,S -isomer shows no ground-state absorbance at this wavelength. Over the next 15 ps, the 360 nm feature reduces in intensity, with only minor changes elsewhere in the spectrum. Dramatic changes occur from 15 to 2800 ps, where the absorption at $\lambda > 600$ nm collapses to zero, thus indicating conversion from a triplet excited-state potential energy surface to a singlet ground-state potential energy surface. The 360 nm feature reduces in intensity concomitant with a rise of the absorption near 500 nm, with the appearance of an isosbestic point near 600 nm. The 2800 ps transient spectrum (bold black trace, Figure 1d) and the ground-state difference spectrum (black trace, Figure 1a) are similar in that both show an intense absorption at ~ 500 nm ascribed to the bis- O -bonded isomer. However, the absorption near 400 nm in the 2800 ps transient is not duplicated in the ground-state difference spectrum. This

may be due to the proximity of the laser line, or, more likely, is due to the formation of the single isomerization product, namely the S,O -isomer (see below). The appearance of the isosbestic point in the 65–2800 ps transient spectra indicates transition of a complex in the ³MLCT state with S -bonded coordination to a singlet GS with O -bonded coordination without the formation of a ground-state intermediate. These data strongly suggest that both $S \rightarrow O$ isomerizations are triggered by a single-photon absorption.

A combination of single wavelength and global fitting analyses were employed to reveal dynamics and isomerization kinetic data. Global analysis yields two lifetimes of 1.64 ± 0.14 and 233.4 ± 6.9 ps. On the basis of our previous studies, we assign the 1.64 ps kinetic phase to formation of an isomerizing ³MLCT state, which features a geometry poised for isomerization.⁵⁶ We ascribe the long component to formation of the both ground-state isomers (S,O and O,O) from a triplet excited-state surface. The nature of this surface and this kinetic component will be discussed later. The single wavelength kinetics are consistent with the global fitting results. We chose to fit the data at four wavelengths: 340, 630, 450, and 606 nm. These first two wavelengths, 340 and 630 nm, correspond to the reduced bpy $\pi^* \rightarrow \pi^*$ transition and to the bpy $\pi \rightarrow \text{Ru}^{3+} d\pi$ transition, respectively, both of the ³MLCT excited state. This latter wavelength (630 nm) features essentially no absorbance from any of the ground-state isomers and thus reports on the excited-state dynamics, as well as the loss of excited state. Due to the stimulated emissions features ranging from ~ 460 to ~ 580 nm, we were unable to obtain reliable kinetic data in this region. Thus, the data at 450 nm report on formation of ground-state S,O -, and O,O -bonded isomers. We also fit data at the isosbestic point (606 nm), which reports on the early time dynamics of the complex, prior to isomerization. These data are displayed in Figures S1–S4. The fit at the isosbestic point reveals a biexponential decay of 1.02 ± 0.3 and 5.0 ± 1.8 ps. The first time constant is consistent with that obtained from the global fit analysis. At present, we do not have an assignment for the 5.0 ps kinetic component, nor do we understand why it is not present in the global analysis. This kinetic trace does not contain the long time kinetic phase corresponding to formation of ground-state products. We fixed the shortest time component (1.0 ps) for the modeling of the kinetic traces at the other wavelengths in order to obtain reliable fits of the data. For 340 nm, a triexponential fit with a fixed 1.0 ps phase revealed time constants of 2.8 ± 1.1 and 250 ± 51 ps. We ascribe the large error for the 250 ps time constant to the poor signal-to-noise ratio at this wavelength. At 450 nm, we found time constants of 5.5 ± 2.0 and 213 ± 8.2 ps. At 630 nm, we found time constants of 4.9 ± 1.8 and 220 ± 29 ps. In accord with the global fitting results, the long time component is assigned to the formation of ground-state S,S -, S,O -, and O,O -bonded isomers from the isomerizing ³MLCT excited state. Surprisingly, neither global fitting nor single-wavelength kinetic fits reveal a short sub-picosecond time constant. This kinetic component is typically attributed to formation of the ³MLCT excited state from the initially populated ¹MLCT excited state and, in closely related [Ru(bpy)₃]²⁺, is known to occur in as short a time as 30 fs.^{57–59} We assume that this transition occurs within the pulse width of our instrument (150 fs). It is striking that the kinetic analysis returns a relatively simple description of a photochemical reaction involving two isomerizations.

The femtosecond transient absorption spectroscopic data of [Ru(bpy)₂(F-bpSO)]²⁺ are qualitatively similar to those

observed for $[\text{Ru}(\text{bpy})_2(\text{OSSO})]^{2+}$. Shown in Figure 2c are the spectral traces collected at different pump–probe delays obtained from magic angle excitation at 355 nm. The data near 355 and 710 nm (wavelength employed to create 355 nm) are omitted for clarity. The 0.75 ps trace exhibits a broad absorption from nearly 500 nm well past 700 nm, which is ascribed to an LMCT transition and a ligand-centered transition of the reduced bipyridine of the $^3\text{MLCT}$ excited state. There are also two excited-state absorption features near 360 and 450 nm. We assign the 360 nm absorption to the intraligand $\pi^* \rightarrow \pi^*$ absorption of the reduced bipyridine, but are uncertain of the origin of the 450 nm transition. There appears to be a relatively weak stimulated emission feature near 500 nm, similar to $[\text{Ru}(\text{bpy})_2(\text{OSSO})]^{2+}$ described above. As time evolves over the next 500 ps, the far visible absorption at 650 nm reduces to zero, concomitant with the appearance of two new ground-state absorption transitions at 400 and 500 nm. Again, the 500 ps transient spectrum (bold black trace, Figure 2c) is in good agreement with the steady-state difference spectrum obtained from the spectral subtraction of the S,S-isomer from the photoproduct generated by bulk photolysis (black trace, Figure 2a). In accordance with the spectral data of $[\text{Ru}(\text{bpy})_2(\text{OSSO})]^{2+}$ and other isomerizing bis-sulfoxides, the 500 nm absorption is assigned to the bis-O-bonded isomer. The more intense 400 nm transition is assigned to a mixed S,O-bonded bis-sulfoxide, where one sulfoxide is S-bonded and the other is O-bonded. Such a species is observed in the photochemical reactivity of $[\text{Ru}(\text{bpy})_2(\text{dmsO})_2]^{2+}$,^{49,52} and $[\text{Os}(\text{bpy})_2(\text{dmsO})_2]^{2+}$ (dmsO = dimethylsulfoxide).⁴⁷ Moreover, we recently discovered the photochemical formation of such an isomer in $[\text{Ru}(\text{bpy})_2(\text{bpSO})]^{2+}$, where bpSO = 1,2-bis(phenylsulfinyl)ethane.⁴⁶ In that study, we demonstrated through pump–repump–probe spectroscopy that each sulfoxide isomerization was triggered sequentially through two separate single-photon absorptions. In contrast, the transient absorption spectra for $[\text{Ru}(\text{bpy})_2(\text{F-bpSO})]^{2+}$ clearly indicate the formation of two isomeric products from a single excitation event, namely S,O- $[\text{Ru}(\text{bpy})_2(\text{F-bpSO})]^{2+}$ and O,O- $[\text{Ru}(\text{bpy})_2(\text{F-bpSO})]^{2+}$.

Similar to $[\text{Ru}(\text{bpy})_2(\text{OSSO})]^{2+}$, single-wavelength and global fitting analyses were performed to characterize the dynamics and isomerization kinetics of $[\text{Ru}(\text{bpy})_2(\text{F-bpSO})]^{2+}$. Triexponential fits were observed at 400 and 600 nm (Figures S5 and S6). These wavelengths correspond to an absorption maximum of the photoisomerization products and to loss of the $^3\text{MLCT}$ excited state, respectively. We were unable to obtain reliable fits at 500 nm, an absorption maximum for the bis-O,O-isomer, due to the stimulated emission features ranging from ~ 475 to ~ 525 nm. Fitting at 400 nm yields lifetimes of 0.23 ± 0.02 , 10.6 ± 0.3 , and 121 ± 25 ps, with similar values obtained at 600 nm. The observed time constants found by global fitting analysis are in good agreement with single-wavelength fits, providing values of 0.45 ± 0.06 , 11.1 ± 1.3 , and 114 ± 60 ps. We ascribe the sub-picosecond component to formation of the $^3\text{MLCT}$ state from the $^1\text{MLCT}$ state, consistent with numerous photophysical reports of $[\text{Ru}(\text{bpy})_3]^{2+}$. The ~ 11 ps kinetic component is assigned to formation of an isomerizing $^3\text{MLCT}$ state, and the longest time component (115–120 ps) is attributed to formation of ground-state S,S-, S,O-, and O,O-isomers, with the S,O- and O,O-isomers displaying new absorption maxima near 400 and 500 nm, respectively.

In order to further test the hypothesis that one absorbed photon yields two isomerizations, we varied the pump intensity

and monitored the absorbance at 500 nm, the absorption maxima of the bis-O-bonded isomers for both complexes. We found a linear correlation (Figures S7 and S8) between the pump intensity (ranging from 300 to 600 μW), which is expected for a one-photon absorption mechanism. Moreover, we do not observe kinetic traces at any wavelength that are consistent with a mechanism in which a ground-state isomer is formed after the initial excitation and is then re-excited. For example, the transient spectra in the red region of the spectrum and resultant kinetic traces illustrate this point. This excited-state absorption is assigned to $\text{bpy } \pi \rightarrow \text{Ru}^{3+} \text{ d}\pi$ LMCT on the basis of literature precedence.^{54,55} Importantly, there is no ground-state absorption at these long wavelengths (~ 650 nm for both compounds, see Figures 1a and 2a) for either of the bis-S-isomers discussed here. Thus, the kinetic changes at these wavelengths are due only to excited-state transformations. That kinetic traces only show a sub-picosecond rise (excited-state formation), followed by a long time decay to zero absorbance (ground state), indicates that all ground-state isomers are formed from the same excited state after the initial excitation. That is, if the bis-O-bonded isomer were formed from two successive photon absorptions from ground-state isomers, then one would expect a kinetic trace with two successive rise (excited-state formation) and fall (ground-state formation) cycles in the red region of the spectrum. The linear power dependence and kinetic traces argue against the absorption of two photons to trigger this photochemistry.

For both compounds, the data indicate that multiple photoproducts formed from phototriggered S \rightarrow O isomerization occur from a single excitation or photon absorption. While the excited-state (MLCT) symmetry of each complex is C_1 (localization of the promoted electron on one bipyridine ligand), the local ground-state symmetry is C_{2v} (see NMR spectra in Supporting Information). In this local symmetry, the σ -bonding framework of the S–Ru–S moiety is formed by an a_1 and b_2 SALC (symmetry-adapted linear combination) with the Ru d_{z^2} and d_{yz} orbitals (the z-axis bisects the S–Ru–S chelate; Figure 3). This simple picture demonstrates that in local C_{2v} (and excited-state C_1 symmetry, though with different

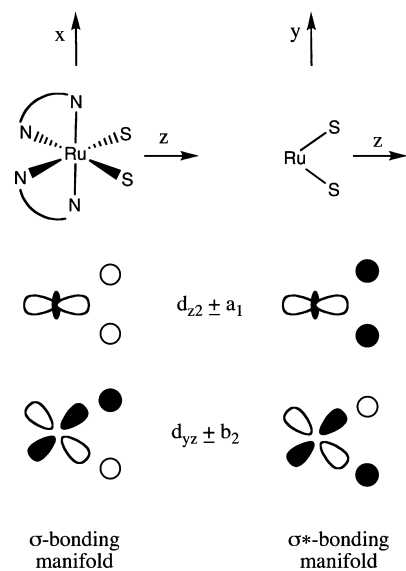
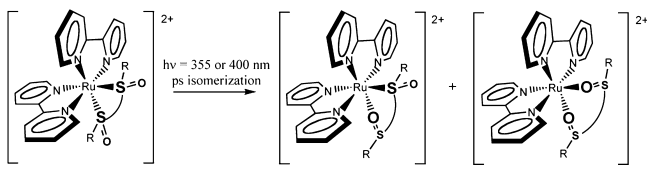


Figure 3. Sketch of orbital interactions depicting the S–Ru–S σ - and σ^* -bonding manifolds.

Mulliken symbols) symmetry, both sulfoxides share common σ -bonding (and antibonding) Ru orbitals, suggesting that two isomerizations from a single-photon absorption is possible. Depopulation of these σ -bonding orbitals or population of their antibonding counterparts will affect both Ru–S bonds simultaneously, but not necessarily to the same degree, due to effects associated with the reduced bipyridine ligand. Thus, if the excited-state potential energy surface contains the σ^* orbital pictured here, then both Ru–S bonds will be broken or weakened upon excitation. Moreover, as the ground-state orbital description involves Ru $d\pi$ stabilization by the sulfoxides (see above), depopulation of these occupied orbitals from light excitation will also weaken both Ru–S bonds. Accordingly, visible light excitation is expected to alter Ru–S bonding through both σ and π interactions. The first molecular events in isomerization must involve Ru–S bond breaking.

One may view this reaction as occurring from an excited-state potential energy surface that permits the formation of multiple photoproducts from sequential isomerizations. From the bonding analysis above, this surface must involve the σ^* -bonding manifold, also known as the ligand field (LF) or metal-centered (MC) states. The surface must also accommodate orthogonal vibrations and nuclear motions involving each sulfoxide isomerization separately. Indeed, the motions leading to the first isomerization will not lead to the second isomerization, though there must exist vibrations common to both isomerizations. Also, the surface must contain contributions from the $^3\text{MLCT}$ state, which is reached upon excitation and triggers both isomerizations (metal oxidation is required for isomerization). Thus, the excited-state potential energy surface that leads to isomerization must involve multiple orthogonal vibrations, comprise both LF (or MC) and MLCT character, and intersect with the ground-state potential energy surface. Such a mechanism suggests the reaction occurs in a non-adiabatic fashion, in which the productive isomerization vibrations are strongly coupled with electronic relaxation from the triplet excited-state surface to the singlet ground-state surface. The intersection of the excited-state surface with the ground-state potential energy surface is more commonly known as a conical intersection seam. The observed product ratio is sensitive to where decay takes place along this seam. Apparently, the conical intersection seams between the ground-state and excited-state potential energy surfaces in $[\text{Ru}(\text{bpy})_2(\text{OSSO})]^{2+}$ and $[\text{Ru}(\text{bpy})_2(\text{F-bpSO})]^{2+}$ are different enough to alter the S,O- to O,O-isomer product ratio (Scheme 1).

Scheme 1. Photochemical Reaction Producing Two Isomers



The spectroscopic data presented here strongly support this interpretation, in particular the observation of isosbestic points connecting spectral features of $^3\text{MLCT}$ excited states with singlet ground states. Indeed, a non-adiabatic isomerization mechanism was found in the computational study of a related photochromic ruthenium sulfoxide compound.² Also, stimulated emission has been observed in certain non-adiabatic

transformations and often accompanies a rapid transition from an excited-state potential energy surface to a ground-state potential energy surface.^{60,61} We observe a red-shifting of the stimulated emission in the early time (0.3–15 ps) transient spectra of $[\text{Ru}(\text{bpy})_2(\text{OSSO})]^{2+}$. This shift is explained as emission from an excited-state surface to a rapidly rising ground-state surface (from loss of Ru $d\pi$ stabilization) in the vicinity of the conical intersection (seam). We suspect that the strong overlap of these signals prevents our clear observation of these effects in the later time spectra (15–2800 ps) of $[\text{Ru}(\text{bpy})_2(\text{OSSO})]^{2+}$ and on any time interval in $[\text{Ru}(\text{bpy})_2(\text{F-bpSO})]^{2+}$.

Another description for the formation of multiple products from sequential isomerizations is from a single, electronic excited state or potential energy surface. For example, excitation of the S,S ground state produces the Franck–Condon states on the $^1\text{MLCT}$ surface. Relaxation to the $^3\text{MLCT}$ surface occurs on the sub-picosecond time scale with S-bonded character, which subsequently yields the isomerizing state or surface in 1–10 ps (Figure 4). As stated above, the reaction pathway from

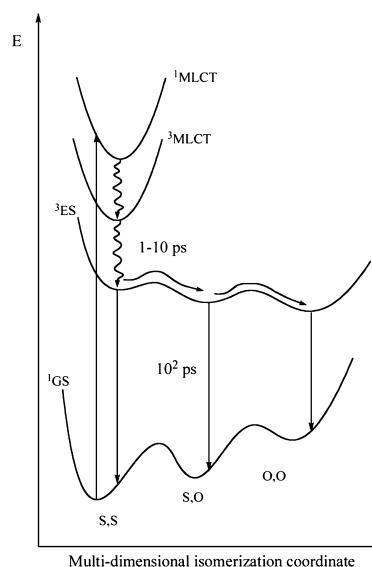


Figure 4. Energy diagram describing photochemical reactivity for $[\text{Ru}(\text{bpy})_2(\text{OSSO})]^{2+}$ and $[\text{Ru}(\text{bpy})_2(\text{F-bpSO})]^{2+}$. The vertical arrows connecting the triplet excited-state surface with the single ground-state surface represent both radiative and nonradiative deactivation pathways.

such a state must involve orthogonal reaction coordinates, as certain of the motions producing the first isomerization are distinct from the second isomerization. That is, once on the triplet excited-state surface, which comprises both LF and MLCT character, the thermodynamic barriers for atomic rearrangement are small ($\Delta H^\ddagger < k_B T$), indicating that largely different structures can be accessed with little energy required to reach a new conformation. Thus, all three isomeric structures on the excited-state surface are in fast equilibrium in comparison to decay to the ground-state potential energy surface. We strongly suspect that these isomerizations are kinematically coupled (lowering the energy barrier between isomers), but these data do not address this hypothesis. In contrast, the ground-state potential energy surface, which allows formation of the S,S-isomer through sequential isomerizations from the O,O-isomer, shows large thermodynamic

barriers between these isomers. Such an observation is consistent with the observed slow thermal reversion rates at room temperature. This mechanism does not require that both isomerizations occur in a concerted or simultaneous fashion; rather, both isomerizations must occur from the triplet excited-state surface.

There are few ultrafast studies of structural rearrangements in transition metal complexes. The recent results of Cu(I) diimine compounds are relevant in that they feature a flattening of the angle formed from two diimine complexes from 90° to 68° with a time constant of 10–15 ps, which is surprisingly independent of diimine and solvent.^{62,63} We have recently observed a solvent dependence on our isomerization, but not on the internal conversion (IC) process involving two separate ³MLCT states.⁴² Woike and co-workers reported from optical transient absorption spectroscopy an isomerization time constant of 300 ± 20 fs in sodium nitroprusside (Na₂[Fe(CN)₅(NO)]) crystals, where NO rotates from N-bonded to side-on NO (η^2).⁶⁴ These measurements are consistent with time-resolved IR studies.⁶⁵ The studies on copper and iron both involve a strong role for the Jahn–Teller distortion in the structural rearrangement or isomerization. Finally, the elongation of Fe–N bonds in light-induced spin-crossover compounds is on the order of 150 fs as measured by a variety of optical and X-ray techniques.⁶⁶ These examples, in conjunction with our studies, demonstrate that a variety of large-amplitude motions can occur on very short time scales.

These results on ruthenium bis-sulfoxides represent a current optimization in excited-state nuclear rearrangements triggered by visible light irradiation as well as in storage of potential energy from photonic energy. Both of these parameters are important in the design of photoactive materials for phototropic or photomechanical effects as well as in photo-origami constructions. The more efficiently a complex (or material) can absorb light and transduce this energy to specific structural and shape deformations, the greater the utility of the complex. Similarly, the efficiency of solar thermal energy storage is predicated on maximizing the conversion of photonic energy to potential energy, which is stored in chemical bonds. For these bis-sulfoxide compounds, one photon leading to two isomerizations indicates more energy is stored per absorbed photon. That we have observed these results in two separate complexes suggests that the unusual reactivity described here may be more general than originally expected. The goal of future studies is to further investigate these and related complexes to help understand the coupling of large atomic displacements with electronic transitions in excited-state reactions.

EXPERIMENTAL SECTION

The starting materials (RuCl₃·xH₂O) and silver hexafluorophosphate (AgPF₆) were purchased from Strem. The reagents 2-fluorothiophenol, 1,2-dibromoethane, and 3-chloroperoxybenzoic acid (*m*CPBA) were purchased from Sigma-Aldrich. ACS-grade solvents were purchased from Fisher Scientific and used without further purification. The starting material Ru(bpy)₂Cl₂·2H₂O was produced in accord with the literature procedure.⁵¹ One of the dithioether ligands (dimethyl bis(dimethylthiomethylene)silane, SS) was received as a gift from Dr. Rabinovich at UNC-Charlotte.

The details of our transient absorption instrumentation have been described elsewhere.⁵⁶ Briefly, Ultrafast transient absorption data were collected using an Ultrafast Systems HELIOS spectrometer, pumped by a Spectra Physics Solstice containing a one-box regenerative amplifier, Mai Tai fs oscillator and an Empower pump laser. Light from the Solstice is split (50:50) to produce pulses of 800 nm (1 kHz,

3.5 W) where one beam is directed to a Light Conversion TOPAS-C OPA to generate the pump beam used in the experiment, and the other beam is used to generate the white light continuum (~330–850 nm) probe beam by passing the 800 nm pulse through a CaF₂ crystal. The probe beam is ~0.2 mm in diameter, and slightly smaller than the pump beam diameter. Typical pump beam power at the sample ranges from 200 to 600 μW. Each spectrum was integrated for 2 s, and the sample was flowed through a fluid pump (Lab Pump Jr., model RHSY by Fluid Metering, Inc., Syosset, NY) flowing at ~7.5 mL/min. Transient data were corrected using Surface Explorer Pro 1.1.5 software (Ultrafast Systems) by subtracting spectral background features that persisted from the previous pulse and appeared pre-pulse, and applying chirp and *t*₀ corrections. For magic angle excitation experiments, the pump beam was directed through a polarizer (Thor Laboratories WPH10M) set in an optical mount and rotated to 18.2°.

[Ru(bpy)₂(SS)](PF₆)₂. The complex Ru(bpy)₂Cl₂·2H₂O (50 mg, 0.096 mmol), dithioether (SS, 20 μL, 0.108 mmol), and AgPF₆ (52.1 mg, 0.02 mmol) were dissolved in 50 mL of 1,2-dichloroethane and refluxed for 3 h under N₂ atmosphere. The solution changed color from purple to deep red, and the precipitation of AgCl occurred. The solution was stored in the refrigerator overnight to induce complete precipitation of AgCl and was filtered by using a fine frit. The filtrate solution was evaporated and then washed with diethyl ether. The resulting red solid product was isolated via vacuum filtration, washed with diethyl ether (3 × 15 mL), and air-dried. Yield: 63 mg (75%). UV–vis (CH₃CN): λ_{max} = 422 nm. ¹H NMR (CD₂Cl₂, 300 MHz): δ (ppm) = 9.63 (d, bpy, 2 H), 8.53 (d, bpy, 2 H), 8.38 (m, bpy, 4 H), 8.0 (m, bpy, 4 H), 7.43 (d, bpy, 2 H), 7.39 (t, bpy, 2 H), 1.92 (d, CH₂, 2 H), 1.85 (d, CH₂, 2 H), 1.2 (s, SCH₃, 6 H), 0.42 (s, SiCH₃, 6 H). ¹³C NMR (CD₃CN, 75 MHz): δ (ppm) = 158.7 (bpy), 157.5 (bpy), 153.4 (bpy), 152.2 (bpy), 139.9 (bpy), 139.7 (bpy), 129.3 (bpy), 128.6 (bpy), 126.0 (bpy), 125.4 (bpy), 20.8 (SCH₂), 20.7 (SCH₃), 2.8 (SiCH₃). Elemental analysis (%), calcd for [RuC₂₆H₃₂F₁₂N₄P₂S₂Si]: C, 35.33; H, 3.65; N, 6.34. Found: C, 35.69; H, 3.79; N, 6.50.

[Ru(bpy)₂(OSSO)](PF₆)₂. Oxidation of [Ru(bpy)₂(SS)](PF₆)₂ was achieved by dissolving [Ru(bpy)₂(SS)](PF₆)₂ (50 mg, 0.0577 mmol) and *m*CPBA (21.5 mg, 0.115 mmol) in 30 mL of acetonitrile. The reaction was allowed to stir at room temperature in the dark for 3 h, and the progress of the reaction was observed by the blue shift of MLCT transition in the UV–vis spectrum. The solution was evaporated and reduced to <5 mL, and the product was isolated by addition of diethyl ether. The yellow colored product was isolated by vacuum filtration, washed with diethyl ether, and air-dried. Yield: 45 mg (90%). UV–vis (CH₃CN): λ_{max} = 355 nm. IR (KBr pellet): S-bonded, ν_{asym}(SO) = 1072 cm⁻¹, ν_{sym}(SO) = 1022 cm⁻¹; O-bonded, ν_{asym}(SO) = 986 cm⁻¹, ν_{sym}(SO) = 935 cm⁻¹. ¹H NMR (CD₃CN, 300 MHz): δ (ppm) = 10.05 (d, bpy, 2 H), 8.56 (d, bpy, 2 H), 8.45 (d, bpy, 2 H), 8.38 (t, bpy, 2 H), 8.13 (t, bpy, 2 H), 7.98 (t, bpy, 2 H), 7.44 (t, bpy, 2 H), 7.25 (d, bpy, 2 H), 3.43 (d, CH₂, 2 H), 2.75 (d, CH₂, 2 H), 2.11 (s, SCH₃, 6 H), 0.53 (s, SiCH₃, 6 H). ¹³C NMR (CD₃CN, 75 MHz): δ (ppm) = 157.8 (bpy), 156.4 (bpy), 155.9 (bpy), 151.2 (bpy), 141.9 (bpy), 141.7 (bpy), 130.4 (bpy), 129.8 (bpy), 126.8 (bpy), 126.1 (bpy), 44.2 (SCH₂), 15.6 (SCH₃), -0.48 (SiCH₃). Elemental analysis (%), calcd for [RuC₂₆H₃₂F₁₂N₄P₂O₂Si]: C, 34.10; H, 3.52; N, 6.12. Found: C, 34.58; H, 3.60; N, 6.40.

1,2-Bis(2-fluorophenylthio)ethane (F-bpte). The starting material 2-fluorothiophenol (2.6160 g, 20.41 mmol) was magnetically stirred with sodium hydroxide (1.1610 g, 29.03 mmol) at room temperature for 30 min in 25 mL of methanol. Solvent was removed by rotary evaporation, and the resulting white solid was redissolved in 25 mL of acetone, after which 1,2-dibromoethane (1.6677 g, 8.88 mmol) was added, and the reaction mixture was brought to reflux while stirring for 4 h. The reaction mixture was cooled to room temperature and filtered. Solvent was removed from the filtrate by rotary evaporation; the resulting white solid was dissolved in 25 mL of toluene and washed with two 20 mL portions of water. The organic phase was dried over magnesium sulfate, and solvent was removed by rotary evaporation. The resultant thin, pale yellow oil was dried on a Schlenk line overnight to yield a pale yellow solid. Yield: 667.5 mg

(26.6%). ^1H NMR (acetone- d_6 , 300 MHz): δ (ppm) = 7.43 (t, 2 H), 7.34 (m, 2 H), 7.18 (t, 4 H), 3.18 (s, 4 H).

[Ru(bpy) $_2$ (F-bpte)](PF $_6$) $_2$. The difluorophenyl dithioether ruthenium complex was synthesized in a manner similar to that used for [Ru(bpy) $_2$ (bpte)](PF $_6$) $_2$. For this synthesis, Ru(bpy) $_2$ Cl $_2$ ·2H $_2$ O (399.9 mg, 0.77 mmol), AgPF $_6$ (392.4 mg, 1.55 mmol), and F-bpte (449.2 mg, 1.60 mmol) were used. After 3 h, additional AgPF $_6$ (191.5 mg, 0.76 mmol) was added. The reaction was allowed to continue for an additional 2 h, at which time the reaction mixture was moved to a freezer to facilitate the complete precipitation of AgCl overnight. The precipitate was removed by filtration through a fine frit, and solvent was removed from the filtrate by rotary evaporation. After being precipitated from a concentrated solution in methanol by the addition of a saturated aqueous solution of NH $_4$ PF $_6$, the ruthenium complex was recrystallized twice from methanol using diethyl ether to precipitate a bright yellow powder. Yield: 0.5238 g (69.2%). UV-vis (PC): λ_{max} = 388 nm. ^1H NMR (acetone- d_6): δ (ppm) = 9.80 (d, bpy, 2 H), 8.39 (t, bpy, 4 H), 8.28 (t, bpy, 2 H), 8.14 (t, bpy, 2 H), 8.04 (m, bpy, 4 H), 7.52 (t, bpy, 2 H), 7.42 (m, F-bpte, 2 H), 6.94 (m, F-bpte, 4 H), 6.85 (t, F-bpte, 2 H), 4.19 (d, CH $_2$, 2 H), 3.64 (d, CH $_2$, 2 H). Elemental analysis (%), calcd for [Ru(C $_{10}$ H $_8$ N $_2$) $_2$ (C $_{14}$ H $_{12}$ F $_2$ S $_2$)](PF $_6$) $_2$ ·2H $_2$ O: C, 39.97; H, 3.16; N, 5.48. Found: C, 39.95; H, 3.02; N, 5.43.

[Ru(bpy) $_2$ (F-bpSO)](PF $_6$) $_2$. Oxidation of [Ru(bpy) $_2$ (F-bpte)] $^{2+}$ (51.3 mg, 0.052 mmol) was achieved by the method previously described.⁴⁶ Upon completion of the oxidation (monitored by UV-vis), the product was precipitated by the addition of diethyl ether, and the precipitate was filtered on a fine frit. The product was mixed with approximately 3 mL of DCM in a small vial and brought to ambient temperature in a freezer. The remaining solid was filtered on a fine frit. This process was repeated twice to yield the pure product. Yield: 38.5 mg (75.0%). UV-vis (PC): λ_{max} = 338 nm. IR (KBr pellet): S-bonded, $\nu_{\text{asym}}(\text{SO}) = 1101 \text{ cm}^{-1}$, $\nu_{\text{sym}}(\text{SO}) = 1085 \text{ cm}^{-1}$; O-bonded, $\nu_{\text{asym}}(\text{SO}) = 960 \text{ cm}^{-1}$, $\nu_{\text{sym}}(\text{SO}) = 937 \text{ cm}^{-1}$. ^1H NMR (acetone- d_6): δ (ppm) = 10.01 (d, bpy, 2 H), 8.49 (t, bpy, 4 H), 8.45 (m, bpy, 2 H), 8.30 (t, bpy, 2 H), 8.13 (t, bpy, 2 H), 7.79 (d, bpy, 2 H), 7.68 (m, bpy/F-bpSO, 4 H), 7.23 (m, F-bpSO, 4 H), 7.04 (m, F-bpSO, 2 H), 5.12 (d, CH $_2$, 2 H), 4.78 (d, CH $_2$, 2 H). Elemental analysis (%), calcd for [Ru(C $_{10}$ H $_8$ N $_2$) $_2$ (C $_{14}$ H $_{12}$ F $_2$ O $_2$ S $_2$)](PF $_6$) $_2$: C, 40.13; H, 2.77; N, 5.50. Found: C, 40.12; H, 3.02; N, 5.68.

■ ASSOCIATED CONTENT

● Supporting Information

NMR spectra and kinetic data. This material is available free of charge via the Internet at <http://pubs.acs.org>.

■ AUTHOR INFORMATION

Corresponding Author

rackj@ohio.edu

Author Contributions

[‡]K.G. and A.W.K. contributed equally.

Notes

The authors declare no competing financial interest.

■ ACKNOWLEDGMENTS

This material is based upon work supported by the National Science Foundation under Grants CHE 0809699, 0947031, and 1112250.

■ REFERENCES

- (1) Bearpark, M. J.; Boggio-Pasqua, M.; Robb, M. A.; Ogliaro, R. *Theor. Chem. Acc.* **2006**, *116*, 670.
- (2) Gottle, A. J.; Dixon, I. M.; Alary, F.; Heully, J. L.; Boggio-Pasqua, M. *J. Am. Chem. Soc.* **2011**, *133*, 9172.
- (3) Indelli, M. T.; Carli, S.; Ghirelli, M.; Chiorboli, C.; Ravaglia, M.; Garavelli, M.; Scandola, F. *J. Am. Chem. Soc.* **2008**, *130*, 7286.
- (4) Boggio-Pasqua, M.; Bearpark, M. J.; Hunt, P. A.; Robb, M. A. *J. Am. Chem. Soc.* **2002**, *124*, 1456.

(5) Boggio-Pasqua, M.; Bearpark, M. J.; Robb, M. A. *J. Org. Chem.* **2007**, *72*, 4497.

(6) Boggio-Pasqua, M.; Ravaglia, M.; Bearpark, M. J.; Garavelli, M.; Robb, M. A. *J. Phys. Chem. A* **2003**, *107*, 11139.

(7) Celani, P.; Bernardi, F.; Olivucci, M.; Robb, M. A. *J. Am. Chem. Soc.* **1997**, *119*, 10815.

(8) Gomez, I.; Reguero, M.; Robb, M. A. *J. Phys. Chem. A* **2006**, *110*, 3986.

(9) Nakamura, S.; Yokojima, S.; Uchida, K.; Tsujioka, T.; Goldberg, A.; Murakami, A.; Shinoda, K.; Mikami, M.; Kobayashi, T.; Kobatake, S.; Matsuda, K.; Irie, M. *J. Photochem. Photobiol. A* **2008**, *200*, 10.

(10) Sanchez-Lozano, M.; Estevez, C. M.; Hermida-Ramon, J.; Serrano-Andres, L. *J. Phys. Chem. A* **2011**, *115*, 9128.

(11) Tomasello, G.; Ogliaro, F.; Bearpark, M. J.; Robb, M. A.; Garavelli, M. *J. Phys. Chem. A* **2008**, *112*, 10096.

(12) Martinez, T. J. *Nature* **2010**, *467*, 412.

(13) Robb, M. A.; Bernardi, F.; Olivucci, M. *Pure Appl. Chem.* **1995**, *67*, 783.

(14) Yarkony, D. R. *Rev. Mod. Phys.* **1996**, *68*, 985.

(15) Yarkony, D. R. *J. Phys. Chem. A* **2001**, *105*, 6277.

(16) Domcke, W.; Yarkony, D. R. *Annu. Rev. Phys. Chem.* **2012**, *63*, 325.

(17) Levine, B. G.; Martinez, T. J. *Annu. Rev. Phys. Chem.* **2007**, *58*, 613.

(18) Matsika, S.; Krause, P. *Annu. Rev. Phys. Chem.* **2011**, *62*, 621.

(19) Yarkony, D. R. *Acc. Chem. Res.* **1998**, *31*, 511.

(20) Balzani, V.; Creedi, A.; Venturi, M. *Chem. Soc. Rev.* **2009**, *38*, 1542.

(21) Bonnet, S.; Collin, J.-P. *Chem. Soc. Rev.* **2008**, *37*, 1207.

(22) Feringa, B. L. *J. Org. Chem.* **2007**, *72*, 6635.

(23) Saha, S.; Stoddart, J. F. *Chem. Soc. Rev.* **2007**, *36*, 77.

(24) Lee, K. M.; White, T. J. *Macromolecules* **2012**, *45*, 7163.

(25) Shimamura, A.; Priimagi, A.; Mamiya, J.; Ikeda, T.; Yu, Y. L.; Barrett, C. J.; Shishido, A. *ACS Appl. Mater. Interfaces* **2011**, *3*, 4190.

(26) Morimoto, M.; Irie, M. *J. Am. Chem. Soc.* **2010**, *132*, 14172.

(27) Zhu, L.; Al-Kaysi, R. O.; Bardeen, C. J. *J. Am. Chem. Soc.* **2011**, *133*, 12569.

(28) Allampally, N. K.; Stassert, C. A.; De Cola, L. *Dalton Trans.* **2012**, *41*, 13132.

(29) Liu, D.; Bastiaansen, C. W. M.; den Toonder, J. M. J.; Broer, D. J. *Macromolecules* **2012**, *45*, 8005.

(30) Pieroni, O.; Fissi, A.; Angelini, N.; Lenci, F. *Acc. Chem. Res.* **2001**, *34*, 9.

(31) Koshima, H.; Ojima, N.; Uchimoto, H. *J. Am. Chem. Soc.* **2009**, *131*, 6890.

(32) O'Bryan, G.; Wong, B. M.; McElhanon, J. R. *ACS Appl. Mater. Interfaces* **2010**, *2*, 1594.

(33) Toshchevikov, V.; Saphiannikova, M.; Heinrich, G. *J. Phys. Chem. A* **2012**, *116*, 913.

(34) Kucharski, T. J.; Tian, Y.; Akbulatov, S.; Boulatov, R. *Energy Environ. Sci.* **2011**, *4*, 4449.

(35) Moth-Poulsen, K.; Coso, D.; Borjesson, K.; Vinokurov, N.; Meier, S. K.; Majumdar, A.; Vollhardt, K. P. C.; Segalman, R. A. *Energy Environ. Sci.* **2012**, *5*, 8534.

(36) Kolpak, A. M.; Grossman, J. C. *Nano Lett.* **2011**, *11*, 3156.

(37) Saltiel, J.; Bremer, M. A.; Laohasurayotin, S.; Krishna, T. S. R. *Angew. Chem., Int. Ed.* **2008**, *47*, 1237.

(38) Saltiel, J.; Papdimtriou, D.; Krishna, T. S. R.; Huang, Z.-N.; Krishnamoorthy, G.; Laohasurayotin, S.; Clark, R. J. *Angew. Chem., Int. Ed.* **2009**, *48*, 8082.

(39) McClure, B. A.; Rack, J. J. *Eur. J. Inorg. Chem.* **2010**, 3895.

(40) Rack, J. J. *Z. Kristallogr.* **2008**, *223*, 356.

(41) Rack, J. J. *Coord. Chem. Rev.* **2009**, *253*, 78.

(42) Garg, K.; Engle, J. T.; Ziegler, C. J.; Rack, J. J. *Chem.—Eur. J.* **2013**, *19*, 11686.

(43) McClure, B. A.; Abrams, E. R.; Rack, J. J. *J. Am. Chem. Soc.* **2010**, *132*, 5428.

(44) McClure, B. A.; Rack, J. J. *Angew. Chem., Int. Ed.* **2009**, *48*, 8556.

- (45) McClure, B. A.; Mockus, N. V.; Butcher, D. P.; Lutterman, D. A.; Turro, C.; Petersen, J. L.; Rack, J. J. *Inorg. Chem.* **2009**, *48*, 8084.
- (46) King, A. W.; Jin, Y.; Engle, J. T.; Ziegler, C. J.; Rack, J. J. *Inorg. Chem.* **2013**, *52*, 2086.
- (47) Mockus, N. V.; Petersen, J. L.; Rack, J. J. *Inorg. Chem.* **2006**, *45*, 8.
- (48) Mockus, N. V.; Rabinovich, D.; Petersen, J. L.; Rack, J. J. *Angew. Chem., Int. Ed.* **2008**, *47*, 1458.
- (49) Rack, J. J.; Mockus, N. V. *Inorg. Chem.* **2003**, *42*, 5792.
- (50) Rachford, A. A.; Petersen, J. L.; Rack, J. J. *Dalton Trans.* **2007**, 3245.
- (51) Sullivan, B. P.; Salman, D. J.; Meyer, T. J. *Inorg. Chem.* **1978**, *17*, 3334.
- (52) Smith, M. K.; Gibson, J. A.; Young, C. G.; Broomhead, J. A.; Junk, P. C.; Keene, F. R. *Eur. J. Inorg. Chem.* **2000**, 1365.
- (53) Dobson, J. C.; Meyer, T. J. *Inorg. Chem.* **1988**, *27*, 3283.
- (54) Damrauer, N. H.; McCusker, J. K. *J. Phys. Chem. A* **1999**, *103*, 8440.
- (55) Braterman, P. S.; Song, J.-I.; Peacock, R. D. *Inorg. Chem.* **1992**, *31*, 555.
- (56) McClure, B. A.; Rack, J. J. *Inorg. Chem.* **2011**, *50*, 7586.
- (57) Bhasikuttan, A. C.; Suzuki, M.; Nakashima, S.; Okada, T. *J. Am. Chem. Soc.* **2002**, *124*, 8398.
- (58) Damrauer, N. H.; Cerullo, G.; Yeh, A.; Boussie, T. R.; Shank, C. V.; McCusker, J. K. *Science* **1997**, *275*, 54.
- (59) Yoon, S.; Kukura, P.; Stuart, C. M.; Mathies, R. A. *Mol. Phys.* **2006**, *104*, 1275.
- (60) Polli, D.; Altoe, P.; Weingart, O.; Spillane, K. M.; Manzoni, C.; Brida, D.; Tomasello, G.; Orlandi, G.; Kukura, P.; Mathies, R. A.; Garavelli, M.; Cerullo, G. *Nature* **2010**, *467*, 440.
- (61) Shim, S.; Joo, T.; Bae, S. C.; Kim, K. S.; Kim, E. J. *J. Phys. Chem. A* **2003**, *107*, 8106.
- (62) Iwamura, M.; Watanabe, H.; Ishii, K.; Takeuchi, S.; Tahara, T. *J. Am. Chem. Soc.* **2011**, *133*, 7728.
- (63) Shaw, G. B.; Grant, C. D.; Shirota, H.; Castner, E. W., Jr.; Meyer, G. J.; Chen, L. X. *J. Am. Chem. Soc.* **2007**, *129*, 2147.
- (64) Schaniel, D.; Nicoul, M.; Woike, T. *Phys. Chem. Chem. Phys.* **2010**, *12*, 9029.
- (65) Galle, G.; Nicoul, M.; Woike, T.; Schaniel, D.; Freysz, E. *Chem. Phys. Lett.* **2012**, *552*, 64.
- (66) Cannizzo, A.; Milne, C. J.; Consani, C.; Gawelda, W.; Bressler, C.; van Mourik, F.; Chergui, M. *Coord. Chem. Rev.* **2010**, *254*, 2677.